Journal of Alloys and Compounds 583 (2014) 162–169

Contents lists available at ScienceDirect

Journal of Alloys and Compounds

journal homepage: www.elsevier.com/locate/jalcom

Microstructure and oxidation behavior of new refractory high entropy alloys

C.M. Liu, H.M. Wang, S.Q. Zhang *, H.B. Tang, A.L. Zhang

Key Laboratory of Aerospace Materials of the Ministry of Education, Beihang University, 37 Xueyuan Road, Beijing 100191, China

ARTICLE INFO

Article history:
Received 11 April 2013
Received in revised form 10 August 2013
Accepted 14 August 2013
Available online 31 August 2013

Keywords:
High entropy alloys
Refractory metal
Microstructure
Oxidation behavior

ABSTRACT

High-entropy alloys (HEAs) are defined as the alloys composed of at least five principal elements in equimolar or near equimolar ratios, which can facilitate the formation of simple solid solutions during solidification. Recent studies suggested that the refractory HEAs exhibited great promise for high temperature structural materials. However, their oxidation behavior had received little attention. In the present study, Cr, Al and Si elements were added to improve the oxidation resistance, four types of new refractory HEAs were designed and synthesized, including $NbCrMoTiAl_{0.5}$ (H-Ti), $NbCrMoVAl_{0.5}$ (H-V), $NbCrMoTiVAl_{0.5}$ (H-TiV) and $NbCrMoTiVAl_{0.5}Si_{0.3}$ (H-$TiVSi_{0.3}$). Their microstructures and oxidation behavior were studied. As expected, these refractory HEAs mainly consist of a simple body-centred cubic (BCC) refractory metal solid solution (RM_{ss}) due to the high mixing entropy effect. Solidification process and thermodynamic analysis were investigated to explain the formation mechanism of their microstructures. For all the refractory HEAs, the oxidation kinetics at 1300 °C follows a linear behavior. The oxidation resistance of the HEAs is significantly improved with Ti and Si addition, but reduced with V addition.

1. Introduction

Refractory metals have the potential to be the next generation of high temperature structural materials because they have high melting points, good performances of high temperature strength and ambient temperature ductility [1–4]. However, their poor oxidation resistance at elevated temperatures limits their application. Considerable works have been performed to solve this problem. It is found that doping high content of Cr, Al and Si elements can cause the formation of protective oxide layers (i.e., Cr_2O_3, Al_2O_3, SiO_2) [5–7]. Unfortunately, at the same time, large quantities of brittle intermetallic compounds (Nb_5Si_3, $NbCr_2$, $MoSi_2$, Nb_3Al, etc.) are easy to form, leading to low fracture toughness at room temperature, which will also restrict their application [8]. This raises the question: can we avoid or reduce the formation of brittle intermetallic compounds when doping some amounts of Cr, Al, Si elements? Furthermore, can the refractory alloys remain ductile solid solution phase? The design idea of new alloy system named "high entropy alloys" (HEAs) may offer a pathway towards solving this problem.

The concept of HEAs is proposed by professor Yeh [9]. The HEAs are composed of at least five principal elements with each elemental concentration between 5 and 35 at.%. The high mixing entropy effect can facilitate the formation of simple solid solutions during solidification instead of brittle intermetallic compounds [9–15]. Recently, NbMoTaW, VNbMoTaW, TaNbHfZrTi refractory HEAs have been successfully produced by vacuum arc melting [3,4,16]. These refractory HEAs consist of single BCC solid solution phase, and are proved to be usable at high temperatures due to their high strength, but studies on their oxidation behavior are limited [17]. Besides, considering that these refractory HEAs contain no Cr, Al, Si elements, their high temperature oxidation resistance should be poor.

Based on the analysis above, high content of Cr, Al and Si elements were added to increase the oxidation resistance [5–7], and the design idea of HEAs was applied to avoid the formation of complex brittle phases. The base composition $NbMoCrAl_{0.5}$ (1:1:1:0.5 in atomic molar ratios) was selected, because Nb metal had good ductility and fracture toughness [18], Mo could increase high temperature strength [1], Cr and Al could improve the oxidation resistance of the alloys [5,6]. Then, four types of new refractory HEAs including $NbCrMoTiAl_{0.5}$ (H-Ti), $NbCrMoVAl_{0.5}$ (H-V), $NbCrMoTiVAl_{0.5}$ (H-TiV) and $NbCrMoTiVAl_{0.5}Si_{0.3}$ (H-$TiVSi_{0.3}$) alloys were designed. Here, H was used to represent $NbMoCrAl_{0.5}$ in this paper to facilitate discussion. The mixing enthalpy between Nb, Mo, V, Cr, Ti refractory elements was small (see Table 1) [19,20]. This was beneficial to the preparation of HEAs [10]. To fully augment the mixing entropy, Nb, Mo, V, Cr and Ti elements were designed in equimolar ratios [9]. But the mixing enthalpy between Al, Si and other elements were more negative, therefore the amount of their addition was relatively low to avoid the formation of intermetallics.

* Corresponding author. Tel./fax: +86 10 8233 9691.
E-mail address: zhangsq@buaa.edu.cn (S.Q. Zhang).

0925-8388/$ - see front matter © 2013 Elsevier B.V. All rights reserved.
http://dx.doi.org/10.1016/j.jallcom.2013.08.102

Table 1
The values of ΔH_{mix} (kJ/mol) calculated by Miedema's model for atomic pairs between elements with Ti, V, Cr, Nb, Mo, Al, Si [19].

Element	V	Cr	Nb	Mo	Al	Si
Ti	−2	−7	2	−4	−30	−66
V		−2	−1	0	−16	−48
Cr			−7	0	−10	−37
Nb				−6	−18	−56
Mo					−5	−35
Al						−19

In this paper, the microstructure and oxidation behavior of these refractory HEAs were investigated with two purposes. One was to verify whether the single phase refractory solid solution with high content of Cr, Al and Si elements can be obtained. The other was to investigate the effect of the alloying elements on the microstructure and oxidation resistance, which would provide a reference for the optimization of the alloy compositions.

2. Experimental

The alloys were prepared from commercial purity (all in 99.9 wt.%) Nb, Cr, Mo, Ti, V, Al and Si by electric arc melting under argon atmosphere in water cooled copper crucible. To prevent the loss of Al and Si, the Nb, Cr, Mo, Ti, V, Al and Si were not added in the copper crucible at the same time during the arc melting. The elements Ti, V, Al and Si were firstly melted, and the first alloy ingot was obtained. Similarly, the Cr, Nb, Mo were melted, and the second alloy ingot were obtained. Then, the final HEAs ingots of about 100 g were prepared by these two alloy ingots. To ensure homogeneity, the alloys were remelted for at least five times.

The crystal structures were characterized using X-ray diffractometer (XRD, Rigaku Dmax 2200) with Cu Kα radiation scanning from 20 to 100 degrees in 2θ at a scanning rate of 6°/min. Microstructures of the cast samples were examined by Cambridge-S360 scanning electron microscopy (SEM) using backscattered electron (BSE) imaging. The chemical compositions of the constituent phases were analyzed by electron-probe microanalysis (EPMA) using a JEOL JXA 8100 super-probe equipped with energy dispersive X-ray (EDX) and wavelength dispersive X-ray (WDX) spectrometers. The precipitate phases were identified by transmission electron microscopy (TEM, JEOL JEM-2100) with thin-foil specimens that were prepared by polished thinning and ion milling. The area fractions of secondary phase in H-Ti and H-TiV alloys were measured using BSE images and the metallographic image analysis software SISC IAS v8.0.

The oxidation coupons with dimensions of approximately 4 mm × 6 mm × 10 mm were ground to 1000 grit and ultrasonically cleaned in ethanol. Isothermal oxidation tests of the samples were undertaken at 1300 °C in air with the exposure times of 5, 10, 15 and 20 h. The weight of samples was examined and recorded. Weight gain per unit area as a function of the time was used to determine the alloy oxidation resistance. The oxidation products were characterized by XRD. The cross-section of the oxide scales was observed and analyzed by EPMA.

3. Results and discussions

In this paper, the microstructures of the HEAs were investigated firstly. To fully understand the formation mechanism of these microstructures, the solidification processes were analyzed, and a simple thermodynamic analysis of the phase formation in each alloy was proposed. Afterwards, the oxidation behavior was studied, and the effect of Ti, V and Si alloying elements on oxidation resistance were discussed.

3.1. Microstructure

The XRD patterns of the refractory HEAs are shown in Fig. 1. As expected, their structure is simple. H-Ti, H-V and H-TiV al loys display a single BCC structure. The H-TiVSi$_{0.3}$ alloy is composed of two phases, including BCC phase and a compound phase (Nb,Ti)$_5$Si$_3$ (JCPDS, 63-3599).

3.1.1. Microstructure characterization

Fig. 2 shows the microstructures of the refractory HEAs. A common observation can be depicted. There is serious dendritic segregation although the matrix is of refractory metal solid solution (RM$_{ss}$) type. Furthermore, except for H-V alloy, all alloys have the secondary phase in interdendritic regions. To facilitate discussion, the microstructures are mainly distinguished as dendrite, interdendrite and secondary-phase regions. Table 2 gives the chemical compositions in each region, which is determined by EDX. It is noticeable that Mo element segregates preferentially to the dendritic regions, while Cr, Ti, Al and Si elements prefer to the interdendritic regions. The distribution of Nb and V elements is relatively homogeneous.

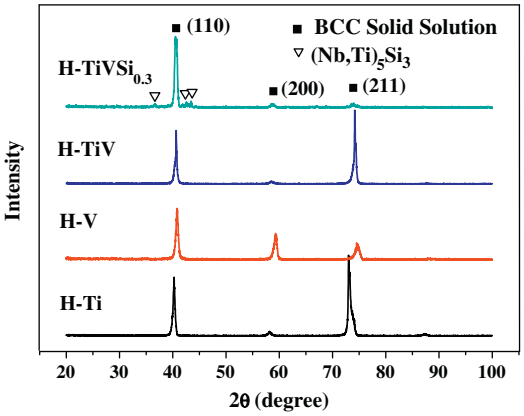

Fig. 1. XRD patterns of the HEAs.

For H-V alloy, it only consists of RM$_{ss}$ as shown in Fig. 2b. For H-TiVSi$_{0.3}$ alloy, it should be the hypoeutectic or hypereutectic microstructure as shown in Fig. 2d. Combining the EDX results and the corresponding XRD patterns (see Fig. 1), it can be summarized that the H-TiVSi$_{0.3}$ alloy consists of RM$_{ss}$ and (Nb,Ti)$_5$Si$_3$ eutectic micro struc ture (see Fig. 2d).

It seems that H-Ti (see Fig. 2a) and H-TiV (see Fig. 2c) exhibit hypomonotectic microstructure. And there are RM$_{ss}$ dendritic and black secondary phase in interdendritic regions. The black secondary phase exhibits irregular or lamellar shape. According to the EDX results in Table 2, the secondary phase is mainly composed of Ti element with the atomic percentage of 71.05% in H-Ti and 79.36% in H-TiV. To further identify the secondary phase, TEM is applied. The selected area diffraction (SAD) (see Fig. 3) pattern analysis indicates that it is a BCC structure with the lattice parameter of about 3.29 Å, very closed to the lattice parameter of the β-Ti solid solution (3.331 Å). Considering its high composition of Ti, it is reasonable to presume that secondary phase is a solid solution of β-Ti. However, β-Ti is not identified in the XRD patterns of H-Ti and H-TiV. This is because that β-Ti has BCC structure and similar lattice parameter with RM$_{ss}$, and has little concentration. Furthermore, the area fraction of β-Ti is measured by differentiating the phases using the BSE contrast. It is found that the area fraction of β-Ti in H-TiV (4.6%) is slightly higher than that in H-Ti (2.5%). This suggests that the addition of V element promotes the formation of β-Ti. This observation of β-Ti is seldom reported. The related reasons will be qualitatively analyzed in Section 3.1.3.

3.1.2. Solidification process

According to Fig. 2a, the H-Ti alloy should be the hypomonotectic microstructure. To better understand it, the hypomonotectic reaction during solidification of H-Ti alloy is schematically illustrated by the phase diagram in Fig. 4, where element A represents the mixture of Nb, Cr, Mo and Al. The solidification path (along the dotted line) of H-Ti can be described as follows: (1) Melting liquid experiences reaction by $L \rightarrow RM_{ss} + L_1$. Primary RM$_{ss}$ form with dendrite growth, and liquid L_1 is left in interdendritic regions, as

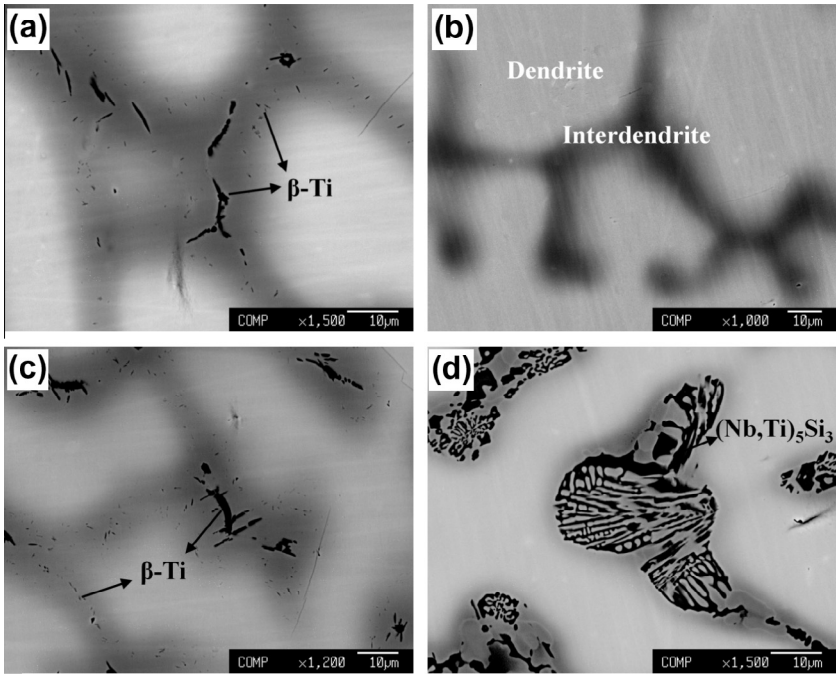

Fig. 2. BSE microstructures of the HEAs: (a) H-Ti, (b) H-V, (c) H-TiV, (d) H-TiVSi$_{0.3}$.

Table 2
Phase constituents and average chemical composition (at.%) for the HEAs studied in this work.

	Nb	Cr	Mo	Al	Ti	V	Si
NbCrMoTiAl$_{0.5}$ (H-Ti)	21.81	24.70	20.01	9.97	23.50		
Dendrite	26.06	14.96	32.03	7.23	19.73		
Interdendrite	20.21	27.06	16.46	11.46	24.81		
β-Ti	8.64	11.56	5.18	3.56	71.05		
NbCrMoVAl$_{0.5}$ (H-V)	22.50	23.04	22.16	10.15		22.15	
Dendrite	22.63	19.10	28.47	7.30		22.50	
Interdendrite	23.25	33.22	10.97	11.22		21.33	
NbCrMoTiVAl$_{0.5}$ (H-TiV)	18.35	18.92	18.08	8.15	18.12	18.38	
Dendrite	19.38	13.41	26.59	5.8	15.85	18.97	
Interdendrite	17.22	23.91	11.55	9.31	17.95	20.06	
β-Ti	5.77	5.01	3.05	1.7	79.36	5.12	
NbCrMoTiVAl$_{0.5}$Si$_{0.3}$ (H-TiVSi$_{0.3}$)	17.68	16.95	17.14	6.96	18.26	17.32	5.69
Dendrite	18.35	14.71	24.98	7.01	14.53	18.71	1.70
Interdendrite	17.18	17.68	7.85	6.91	23.08	15.23	12.07
(Nb,Ti)$_5$Si$_3$	21.69	5.30		4.40	29.28	8.46	30.87

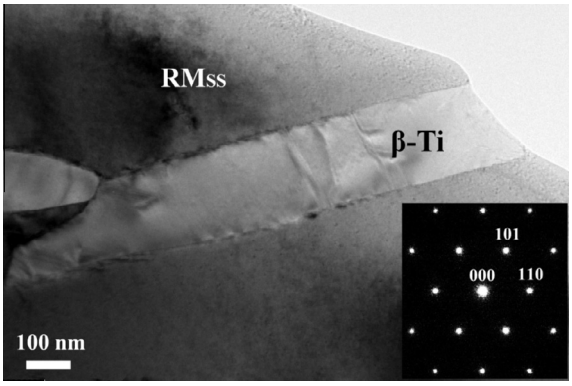

Fig. 3. TEM bright-field image of the H-Ti alloy showing lamellar β-Ti, the corresponding diffraction pattern in the [$\bar{1}$11] zone axis indicating BCC phase (α = 3.29 Å).

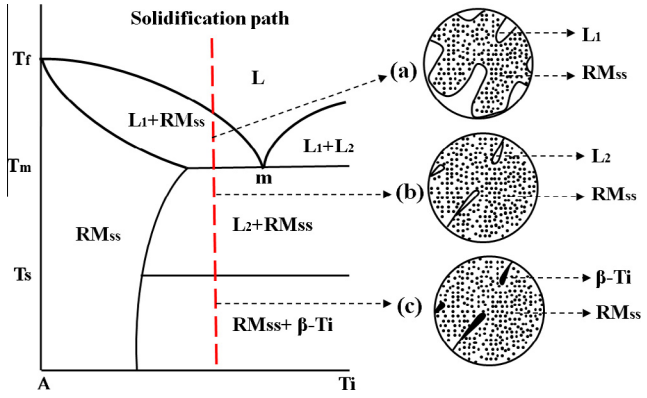

Fig. 4. Phase diagram schematically depicts the hypomonotectic reaction in H-Ti alloy. Here, element A represents the mixture of Nb, Cr, Mo and Al.

Table 3
The microstructures and the parameters Ω and δ for the refractory HEAs. The superscript "*" denotes the empirical criterion for forming solid solution phase [21].

Alloys	Microstructure	δ (%)	Ω
H-Ti	RM_{ss} + β-Ti	5.14	2.50
H-V	RM_{ss}	4.75	3.40
H-TiV	RM_{ss} + β-Ti	5.00	3.30
H-TiVSi$_{0.3}$	RM_{ss} + $(Nb,Ti)_5Si_3$	5.97	1.80
Criterion*		$\leqslant$6.6	$\geqslant$1.1

shown in Fig. 4a. (2) At the temperature T_m, the monotectic reaction $L_1 \rightarrow RM_{ss} + L_2$ occurs. RM_{ss} dendrite will continue to grow, leaving L_2 in interdendritic regions which is the liquid phase of β-Ti solid solution, as shown in Fig. 4b. (3) The reaction $L_2 \rightarrow$ β-Ti takes place until the solidification process completes. β-Ti forms in interdendritic regions and presents irregular shapes, as shown in Fig. 4c. At cooling, little lamellar β-Ti will precipitate in the RM_{ss}. Thus, the solidification process can be summarized as $L \rightarrow RM_{ss} + L_1 \rightarrow RM_{ss} + L_2 \rightarrow RM_{ss}$ + β-Ti. As a result, in H-Ti alloy, the refractory metal solid solution forms as a continuous matrix, whereas the β-Ti distributes discontinuously and retain isolated pockets in the interdendritic regions. The H-TiV alloy has the similar solidification process to that of H-Ti alloy.

Besides, the solidification processes of H-V and H-TiVSi$_{0.3}$ are simple and featureless. H-V is an isomorphous alloy, and its solidification process can be described as $L \rightarrow RM_{ss}$. While H-TiVSi$_{0.3}$ alloy undergoes hypoeutectic or hypereutectic reaction during solidification, and its solidification process can be described briefly as $L \rightarrow RM_{ss} + L_1 \rightarrow RM_{ss} + (Nb,Ti)_5Si_3$.

3.1.3. Thermodynamic analysis of the phase formation

Compared with traditional alloys containing so many component elements, the structure of the refractory HEAs is relatively simple due to the high mixing entropy effect [9,11]. Recently, a few studies have been carried out on the phase formation rule for HEAs [10,21–23]. Based on the work of Yang and Zhang [21], two parameters Ω and δ are defined as follows to predict the solid solution formation for various HEAs:

$$\Omega = \frac{T_m \Delta S_{mix}}{|\Delta H_{mix}|} \tag{1}$$

$$\delta = \sqrt{\sum_{i=1}^{n} c_i \left(1 - \frac{r_i}{\bar{r}}\right)^2} \tag{2}$$

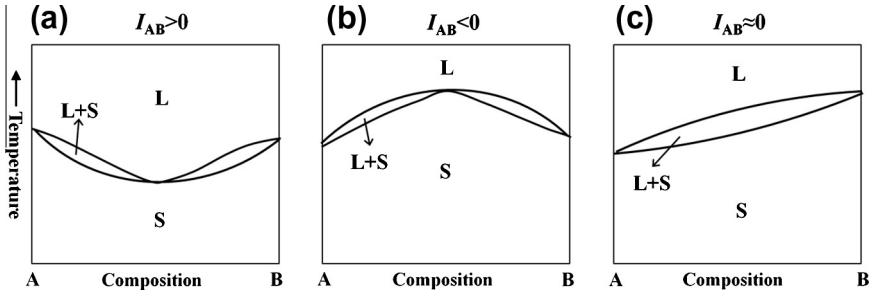

Fig. 5. Schematic binary phase diagrams [24], where the liquidus shows (a) a minimum, when $I_{AB} < 0$, (b) a maximum, when $I_{AB} > 0$, and (c) neither minimum nor maximum, when $I_{AB} = 0$.

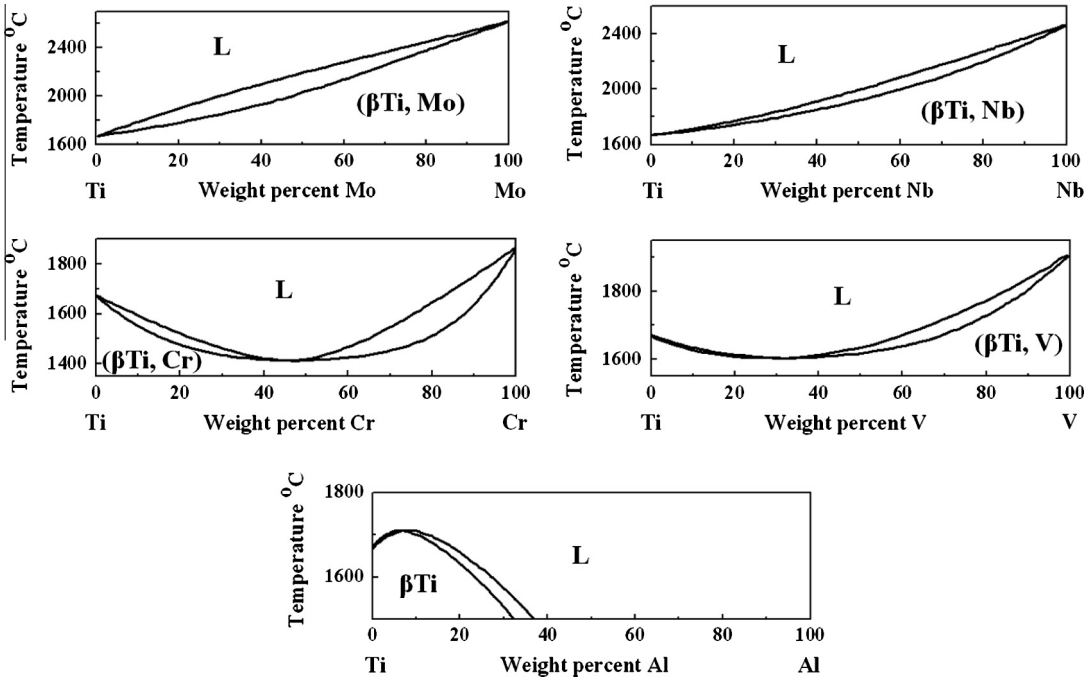

Fig. 6. Schematic illustration for the liquidus and solidus in Ti–Mo, Ti–Nb, Ti–Cr, Ti–V and Ti–Al binary phase diagrams.

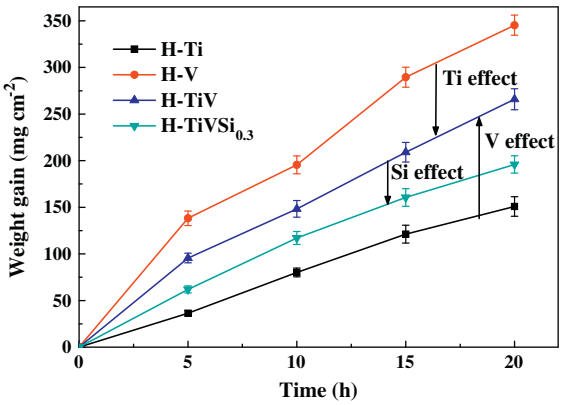

Fig. 7. The isothermal oxidation curves for the HEAs at 1300 °C, showing the effects of Ti, V and Si addition.

where T_m is the melting temperature of HEAs, ΔH_{mix} is the enthalpy of mixing and ΔS_{mix} is the entropy of mixing, c_i is the atomic percentage of the ith component, r_i is the corresponding atomic radius. And $\bar{r}$ is the average atomic radius. The detailed calculation method is the same as that described in Ref. [21].

Larger Ω and smaller δ will facilitate solid-solution formation [21]. For the refractory HEAs considered in this work, parameters Ω and δ are calculated and listed in Table 3. It can be seen that H-V has the largest Ω and smallest δ, and thus it consists of single solid solution. While H-TiVSi$_{0.3}$ has the smallest Ω and largest δ, hence the (Nb,Ti)$_5$Si$_3$ phase forms. Furthermore, an empirical criterion for the HEAs to form solid solution is also suggested by Yang and Zhang. That is, $\Omega \geqslant 1.1$ and $\delta \leqslant 6.6\%$. According to this criterion, all the considered refractory HEAs should have the solid solution structure. But this only holds for H-V, H-Ti and H-TiV alloys. As for H-TiVSi$_{0.3}$ alloy, the (Nb,Ti)$_5$Si$_3$ phase forms. This suggests that this criterion specified for HEAs appears to be necessary but not sufficient enough to predict the solid solution formation in HEAs. The reason for the formation of (Nb,Ti)$_5$Si$_3$ phase should be related with the most negative mixing enthalpy between Nb, Ti and Si elements (see Table 1).

Besides, an intriguing question is why H-Ti and H-TiV alloys undergo a hypomonotectic reaction and yield the β-Ti. It is well known that the monotectic reaction results from the immiscibility of two liquid phases [24]. This suggests that the liquid phase of β-Ti and RM$_{ss}$ may be mutually immiscible. In order to explore the reason for this immiscibility, the interaction between the elements in RM$_{ss}$ and β-Ti should be considered. For binary system, I_{AB} is the regular solution interaction parameter between A and B elements [24,25]. When $I_{AB} > 0$, the liquidus shows a minimum in AB binary phase diagram (see Fig. 5a). The liquid phase of A and B may be mutually immiscible. During solidification, AB alloy may undergo monotectic reaction, or spinodal decomposition and so on. When $I_{AB} < 0$, the liquidus shows a maximum in AB binary phase diagram (see Fig. 5b). AB alloy may generate intermetallics. when $I_{AB} \approx 0$, the liquidus shows neither maximum nor minimum in the AB binary phase diagram (see Fig. 5c), the solid solution will be obtained. Based on the analysis above, element A and element B will become mutually immiscible when $I_{AB} > 0$, and I_{AB} can be qualitatively analyzed according to the shape of the liquidus in binary alloy phase diagrams [26]. Accordingly, the I_{AB} between Nb, V, Mo, Ti, Al and β-Ti can be easily obtained from Fig. 6: $I_{NbTi} \approx 0$, $I_{MoTi} \approx 0$, $I_{TiAl} < 0$, $I_{VTi} > 0$, $I_{CrTi} > 0$. In H-Ti alloy, there are Nb, Mo, Ti, Cr and Al elements. Since only $I_{CrTi} > 0$, it should be Cr that results in the immiscibility between β-Ti and the RM$_{SS}$. For H-TiV, $I_{VTi} > 0$, thus the amount of β-Ti increases due to the addition of V. This also explains why the area fraction of β-Ti in H-TiV (4.6%) is more than that in H-Ti (2.5%). In the previous research about 48Nb–15Cr–37Ti alloy [27], 5.2% β-Ti is deposited from the Nb–Cr–Ti solid solution after holding at 1000 °C for 338 h. Because $I_{NbTi} \approx 0$, element Nb plays negligible role in participating β-Ti. Whereas Cr plays a critical role due to $I_{CrTi} > 0$. This observation of β-Ti verifies our inference. Accordingly, it is reasonable to predict that β-Ti will form in refractory metal solid solution, when the refractory alloys contain high content of Ti and Cr. However, the formation of β-Ti is detrimental for high temperature structural refractory alloys due to the following reasons. The strength of β-Ti is lower than that of RM$_{ss}$ due to

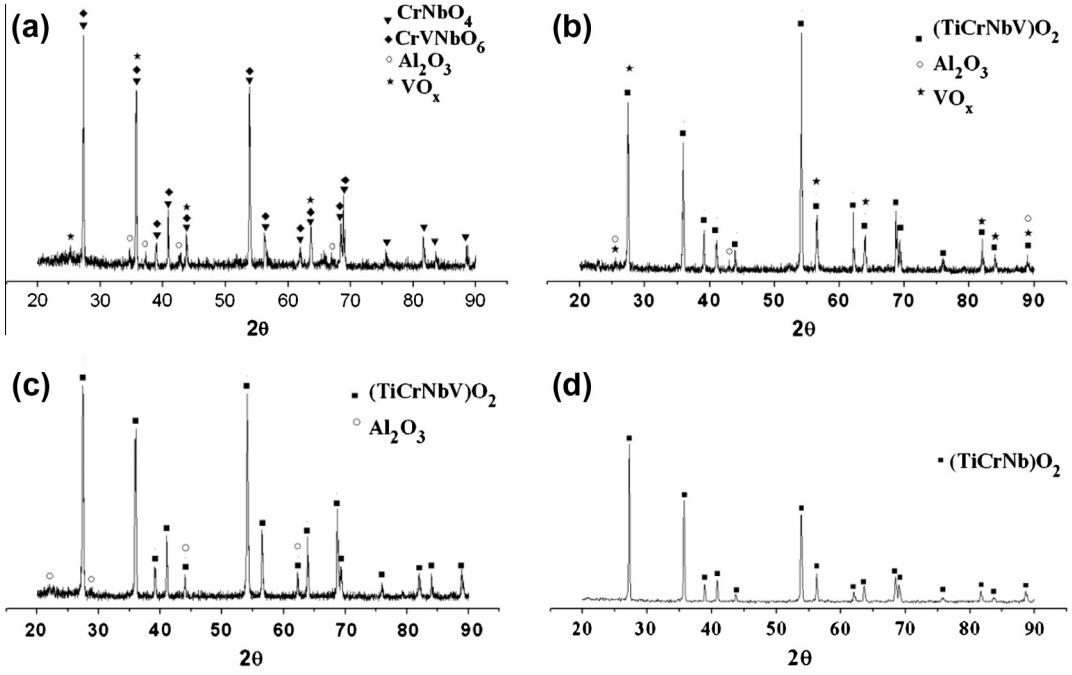

Fig. 8. XRD patterns of the oxidation products obtained after oxidizing the HEAs at 1300 °C for 20 h: (a) H-V, (b) H-TiV, (c) H-TiVSi$_{0.3}$, (d) H-Ti.

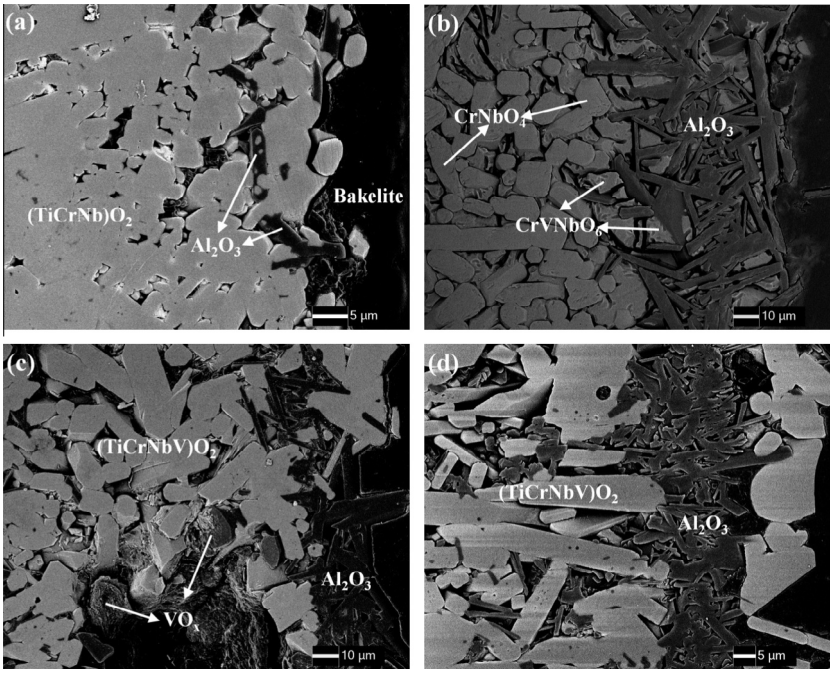

Fig. 9. BSE images showing the cross sections of the outer oxide scales of the HEAs oxidized at 1300 °C for 10 h: (a) H-Ti, (b) H-V, (c) H-TiV, (d) H-TiVSi$_{0.3}$.

the lower solid solution strengthening effect (see Table 2). Meanwhile, the oxidation resistance of β-Ti is also worse than RM$_{ss}$ due to lack of Cr and Al elements. Thus, when designing Nb–Si–Ti–Cr, Nb–Ti–Cr alloys [28–31] and further optimizing the HEAs compositions, the formation of β-Ti should be inhibited by decreasing the content of Ti or Cr.

3.2. Oxidation behavior

Fig. 7 shows the weight gain per unit area as a function of the exposure time at 1300 °C for the HEAs. Results show that all the HEAs exhibit linear oxidation kinetics. Then the linear oxidation rate constant k_1 for each alloy is calculated by the equation $k_1 = \frac{\Delta m}{At}$. Here, Δm is the weight change of the specimen, A is the surface area of the specimen and t is the exposure time. It can be found that H-V alloy exhibits the highest weight gain and hence the worst oxidation resistance. The k_1 is up to 17.3 mg cm^{-2} h^{-1}. Comparatively, the addition of Ti significantly improves the oxidation resistance of H-TiV, and k_1 decreases to 13.3 mg cm^{-2}h^{-1}. When Si is added to H-TiV, H-TiVSi$_{0.3}$ alloy exhibits better oxidation resistance, and k$_1$ decreases to 9.8 mg cm^{-2} h^{-1}. When V element is eliminated from H-TiV, H-Ti alloy has the best oxidation resistance with k$_1$ about 7.5 mg cm^{-2} h^{-1}. These results suggest that the addition of Ti and Si can improve the oxidation resistance, but the addition of V has the opposite effect. To determine the reasons, the oxidation products and the oxide scales are investigated.

Fig. 8 presents the XRD patterns obtained from the oxidation products of the HEAs after exposure at 1300 °C for 20 h. Fig. 9 shows the cross sections of the outer oxide scales of the four HEAs. Table 4 gives the chemical compositions, which are determined by EDX. The oxidation products are determined by the XRD results, the composition information, as well as the oxide morphology. It has been found that CrNbO$_4$ (JCPDS 34-0366) is the predominant oxide in the oxidation products of H-V alloy, and some amount of CrVNbO$_6$ (JCPDS 36-0788) is also present (see Fig. 9b). Besides, V oxides (VO$_x$), including V$_2$O$_5$ (JCPDS 54-0513) and VO$_2$ (JCPDS 76-0676) etc., are found in the oxidation products of H-V and H-TiV alloys (see Fig. 10). When the HEAs contain Ti element, i.e., H-Ti, H-TiV and H-TiVSi$_{0.3}$, TiO$_2$ (JCPDS 76-0321) is the predominant oxide (see Fig. 8). Meanwhile, many other refractory elements are soluted in the TiO$_2$ structure according to the chemical compositions in Table 4. Here, (TiCrNbV)O$_2$ is the predominant oxide of H-TiV and H-TiVSi$_{0.3}$ alloys, and (TiCrNb)O$_2$ is the predominant oxide of H-Ti alloy. In addition, Al$_2$O$_3$ (JCPDS 75-1864) is also observed in all these HEAs in Fig. 9, but it could not be identified by XRD patterns in the oxidation products of H-Ti alloy due to its little concentration.

Several results can be obtained to interpret why V is detrimental, but Si and Ti are beneficial to the oxidation resistance. The effect of V can be discussed from two aspects: (i) The oxides of H-Ti is compact with little porosity (see Fig. 9a). But after V is added, the oxide scales become porous for the other HEAs. This will prompt oxygen ingress towards the metal-oxide interface. (ii) Large size pores are observed in the oxide scales of H-V and H-TiV with the diameter about 50 μm as shown in Fig. 10. And VO$_x$ are observed in the vicinity of the pores. Considering that V$_2$O$_5$ has a low melting point [32], the pores are probability formed due to the fusion or volatilization of the V$_2$O$_5$. These large pores will also prompt oxygen ingress towards the metal-oxide interface, and then increase the oxidation rate. As for Si, the following three aspects can be

Table 4
Average chemical compositions (at.%) of the phases present in the oxide scales obtained after oxidizing the HEAs at 1300 °C for 20 h.

Alloy	Phases	Nb	Cr	Mo	Al	Ti	V	Si	O
H-Ti	(TiCrNb)O$_2$	12.8	11.3		3.6	11.1			61.3
	Al$_2$O$_3$		7.4		31.8	0.4			60.4
H-V	CrNbO$_4$	14.8	14.7		3.5		7.7		59.4
	CrVNbO$_6$	15.9	12.3		1.0		15.0		55.9
	VO$_x$		1.0	9.1	0.6		21.6		67.7
	Al$_2$O$_3$		15.4		31.3		0.5		52.9
H-TiV	(TiCrNbV)O$_2$	12.0	12.2		1.6	10.9	7.8		55.5
	VO$_x$		1.5	9.4	1.5	1.2	30.1		56.4
	Al$_2$O$_3$		10.4		36.7		1.2		51.7
H-TiVSi$_{0.3}$	(TiCrNbV)O$_2$	13.6	11.6		1.7	10.4	8.2	0.5	54.0
	Al$_2$O$_3$		9.9		24.7	0.3	1.7	9.2	54.2

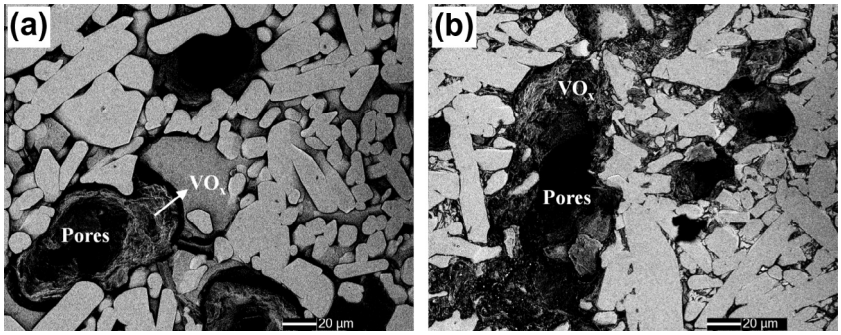

Fig. 10. BSE images showing the large size pores in the oxide scales of the HEAs: (a) H-V, (b) H-TiV.

addressed: (i) In the oxide scales of H-TiVSi$_{0.3}$, there is neither observable large size pores nor VO_x. And the XRD results also indicate the absence of VO_x (see Fig. 8). This suggests that the addition of Si element prevents the formation of VO_x, and hence improves the oxidation resistance. (ii) The $(Nb,Ti)_5Si_3$ phase can act as a significant barrier for the diffusion of oxygen in RM_{ss} [33]. (iii) At the outermost oxide scales of all the HEAs, Al_2O_3 layers are observed. In particular, compared with others, the Al_2O_3 layer in the oxide scales of H-TiVSi$_{0.3}$ is more uniform and compact, and hence more favorable for oxidation resistance. The chemical compositions listed in Table 4 indicate that Si is rich in the Al_2O_3 of the H-TiVSi$_{0.3}$ oxide. It is reasonable to infer that the addition of Si element favors the formation of Al_2O_3. Although the Al_2O_3 layers do not provide an effective barrier to oxidation in the present study, if the optimization of the HEAs compositions can make the Al_2O_3 layers more compact and thicker, the oxidation resistance may be greatly improved. This sheds some light on our further studies. Next, the influence of Ti is discussed as follows. The predominant oxide of H-V is $CrNbO_4$. When Ti is added, the predominant oxide of H-TiV becomes $(TiCrNbV)O_2$. These two oxides have the same crystal structure (see Fig. 8b and c). Meanwhile, the oxide size and morphology are also similar (see Fig. 9b and c). Thus, the oxide scale analysis cannot provide sufficient insight into the effect of Ti addition. As pointed out in the previous study, the addition of Ti can reduce the solid solubility and diffusivity of oxygen in Nb based alloys [34–36], for example, for Nb-25Ti the diffusivity is 1/20 that in pure Nb [37]. This should be the reason why the addition of Ti can improve the oxidation resistance.

4. Conclusions

In this paper, four types of new refractory HEAs were prepared, whose microstructures and oxidation behavior were intensively studied. The main findings could be summarized as follows:

1. H-V alloy consists of single RM_{ss} phase. H-TiVSi$_{0.3}$ exhibits hypoeutectic or hypereutectic microstructure with RM_{ss} and $(Nb,Ti)_5Si_3$ phase. H-Ti and H-TiV alloys probably undergo a hypomonotectic reaction during solidification, yielding the products of RM_{SS} and little β-Ti solid solution. And the β-Ti in H-TiV (4.6%) is more than that in H-Ti (2.5%).
2. Thermodynamic analysis indicates that the formation of $(Nb,Ti)_5Si_3$ is associated with the high negative mixing enthalpy between Si and Nb, Ti. Whereas the immiscibility between β-Ti and Cr, V results in the formation of β-Ti.
3. All the HEAs exhibit linear oxidation kinetics at 1300 °C. Al_2O_3 layers are observed at the outermost oxide scales of all the HEAs. $CrNbO_4$ is the predominant oxide of H-V, while TiO_2 is the predominant oxide of H-Ti, H-TiV and H-TiVS$_{i0.3}$ alloys. Besides, VO_x is also found in oxidation products of the H-V and H-TiV alloys, which results in large size pores in the oxide scales.
4. The alloying elements have a strong influence on the oxidation resistance. The addition of Ti and Si can improve the oxidation resistance, but V is detrimental to oxidation resistance.
5. The present work provides some guidance in the further development of current ideas to obtain refractory high temperature structural materials. Further studies are being carried out to investigate the formation mechanism of the oxidation products, high temperature strength and room temperature fracture toughness of these alloys. Parallel experimental study is also in progress for the optimization of alloy compositions.

Acknowledgements

The work was financially supported by the State Key Basic Research Program of China (Grant No. 2010CB731705). The authors are grateful to Dr. Y.N. Cui at Tsinghua University for helpful discussions.

References

[1] C.L. Ma, J.G. Li, Y. Tan, R. Tanaka, S. Hanada, Mater. Sci. Eng., A 386 (2004) 375–383.
[2] H. Jiang, M. Hirohasi, Y. Lu, H. Imanari, Scr. Mater. 46 (2002) 639–643.
[3] O.N. Senkov, G.B. Wilks, J.M. Scott, D.B. Miracle, Intermetallics 19 (2011) 698–706.
[4] O.N. Senkov, J.M. Scott, S.V. Senkova, D.B. Miracle, C.F. Woodward, J. Alloys Comp. 509 (2011) 6043–6048.
[5] B.G. Kim, G.M. Kim, C.J. Kim, Scr. Mater. 33 (1995) 1117–1125.
[6] K. Zelenitsas, P. Tsakiropoulos, Mater. Sci. Eng., A 416 (2006) 269–280.
[7] M.d.P. Moricca, S.K. Varma, J. Alloys Comp. 489 (2010) 195–201.
[8] K.S. Chan, Mater. Sci. Eng., A 329–331 (2002) 513–522.
[9] J.W. Yeh, Adv. Eng. Mater. 6 (2004) 299–303.
[10] A. Li, X. Zhang, Acta. Metall. Sin. (Eigl. Lett.) 22 (2009) 219–224.
[11] J.H. Pi, Y. Pan, L. Zhang, H. Zhang, J. Alloys Comp. 509 (2011) 5641–5645.
[12] J.H. Pi, Y. Pan, H. Zhang, L. Zhang, Mater. Sci. Eng., A 534 (2012) 228–233.
[13] K.-C. Hsieh, C.-F. Yu, W.-T. Hsieh, W.-R. Chiang, J.S. Ku, J.-H. Lai, C.-P. Tu, C.C. Yang, J. Alloys Comp. 483 (2009) 209–212.
[14] T.T. Shun, C.H. Hung, C.F. Lee, J. Alloys Comp. 495 (2010) 55–58.
[15] A. Manzoni, H. Daoud, S. Mondal, S. van Smaalen, R. Völkl, U. Glatzel, N. Wanderka, J. Alloys Comp. 552 (2013) 430–436.
[16] O.N. Senkov, C.F. Woodward, Mater. Sci. Eng., A 529 (2011) 311–320.
[17] O.N. Senkov, S.V. Senkova, D.M. Dimiduk, C. Woodward, D.B. Miracle, J. Mater. Sci. 47 (2012) 6522–6534.
[18] K. Chan, D. Davidson, Metall. Mater. Trans. A 30 (1999) 925–939.
[19] A. Takeuchi, A. Inoue, Mater. Trans. 46 (2005) 2817–2829.
[20] A. Takeuchi, A. Inoue, Mater. Trans. 41 (2000) 1372–1378.
[21] X. Yang, Y. Zhang, Mater. Chem. Phys. 132 (2012) 233–238.
[22] R. Raghavan, K.C. Hari Kumar, B.S. Murty, J. Alloys Comp. 544 (2012) 152–158.
[23] Y. Zhang, Y.J. Zhou, J.P. Lin, G.L. Chen, P.K. Liaw, Adv. Eng. Mater. 10 (2008) 534–538.
[24] F. Campbell, Phase Diagrams: Understanding the Basics, ASM International, Materials Park, Ohio, 2012.
[25] J. Xu, T.F. Jin, Thermodynamics and Kinetics of Materials, Publishing House of Harbin Institute of Technology, Harbin, 2003.

[26] R.Z. Tang, R.Z. Tian, Binary Alloy Phase Diagrams and Crystal Structure of Intermediate Phase, Central South University Press, Changsha, 2009. pp. 836–1107.
[27] D.L. Davidson, K.S. Chan, Metall. Mater. Trans. A 33 (2002) 401–416.
[28] D.L. Davidson, K.S. Chan, D.L. Anton, Metall. Mater. Trans. A 27 (1996) 3007–3018.
[29] I. Grammenos, P. Tsakiropoulos, Intermetallics 18 (2010) 242–253.
[30] Y.Z. Zhan, Z. Sun, J.C. Jiang, J.B. Ma, X.J. Zhang, Y.H. Zhuang, J. Alloys Comp. 468 (2009) 150–153.
[31] K.S. Chan, Metall. Mater. Trans. A 32 (2001) 2475–2487.
[32] J.A. Dean (Ed.), Lange's Handbook of Chemistry, 16th ed., McGraw-Hill, New York, 1998. p. 161.
[33] B. Xiong, C. Cai, H. Wan, Y. Zheng, J. Alloys Comp. 486 (2009) 330–334.
[34] D.Q. Yi, D. Li, H.Q. Liu, C.P. Wu, H.M. Zhou, J. Iron. Steel Res. Int. 14 (2007) 1–6.
[35] L. Yin, D.Q. Yi, L.R. Xiao, L. Yang, H.Q. Liu, Mater. Prot. 36 (2003) 4–8.
[36] J. Geng, P. Tsakiropoulos, G.S. Shao, Mater. Sci. Eng., A 441 (2006) 26–38.
[37] E.A. Aitken, Intermetallic Compounds, Wiley, New York, 1967. pp. 491–515.